

**2018 NDIA GROUND VEHICLE SYSTEMS ENGINEERING AND TECHNOLOGY
SYMPOSIUM
MATERIALS & ADVANCE MANUFACTURING (M&AM) TECHNICAL SESSION
AUGUST 7-9, 2018 - NOVI, MICHIGAN**

**HIGH MN, HIGH AL STEELS FOR THICK PLATE ARMOR
APPLICATIONS**

**Katherine Sebeck, PhD
Ian Toppler
Matt Rogers
U.S. Army TARDEC
Warren, MI**

**Krista Limmer, PhD
Bryan Cheeseman, PhD
US Army Research Lab
Aberdeen, MD**

**LTC Ryan Howell, PhD
US Army PEO GCS
Warren, MI**

**William Herman, PhD
General Dynamics Land
Systems
Sterling Heights, MI**

ABSTRACT

FeMnAlC alloys exhibit lower density (6.5-7.2 g/cm³) than traditional military steels (7.9 g/cm³) while maintaining similar energy absorption capabilities. Material substitutions in legacy systems must meet existing form/fit/function requirements, limiting opportunities for lightweighting of existing designs. This study examines production and material properties of thick plate with a nominal chemistry of 30% Mn, 9%Al and 1%C, in the wrought condition.

Due to the high aluminum and carbon content, there are unique challenges to large scale (45+ ton heat) production versus typical armor steel chemistries. Lab-scale wrought and production material are characterized, comparing microstructure, and mechanical properties. Processing practices including teeming flux and rolling temperature are discussed. The high manganese content of this alloy presents challenges for welding and machining practices, such as limited compatibility of weld wires and substantial work hardening during many basic fabrication operations. Mechanical property data and micrographs from initial gas metal arc welding and machining are presented and discussed.

MOTIVATION AND BACKGROUND

Across Army ground vehicle platforms, weight continues to increase in response to changing requirements. In some cases, the platforms are now exceeding the capabilities of support systems, affecting transportability, or restricting the ability to incorporate additional upgrades. [1] However, the existing form/fit/function requirements limit solutions for weight reduction. A lightweight FeMnAlC steel with 1:1 ballistic efficiency and a

10-15% density reduction was previously demonstrated for castings and laboratory-scale wrought plate. [2] [3] The objective is to meet the same mechanical and ballistic performance requirements as current armor steels, such as rolled homogenous armor (RHA) steel. This allows weight reduction in legacy platforms without altering interfaces, and this makes FeMnAlC one of the largest potential weight savings opportunities for the Abrams tank. [4]

To date, the majority of work in this general alloy chemistry has focused on thin sheet for automotive or small scale heats (500 lb) produced via vacuum induction melting (VIM) or sand castings. [2] Production of thick plate in quantities appropriate for Army ground vehicles presents additional challenges, both in steel making and integration of material. This steel is fully austenitic and non-magnetic, which can cause issues for handling in some plate production facilities. Welding and machining parameters also must be developed for successful integration into vehicle platforms.

INTRODUCTION

FeMnAl steel has previously been evaluated in the cast form and in wrought form as produced by small-scale methods. [2] Material maturation for armor application must address a number of key areas: manufacturability, ballistic performance, blast performance, weldability, machinability, mechanical characterization for modeling and simulation, and corrosion protection. This paper focuses on the manufacturability and weldability, with some discussion of machinability.

The effort to transition to large scale production is pursuing arc furnace melting and bottom-fill teeming of ingots which will then be hot rolled and aged. There are many parameters which must be evaluated that affect final chemistry, microstructure, surface quality, defects, and overall yield.

Figure 1 shows a typical process flow for production of wrought FeMnAl plate.

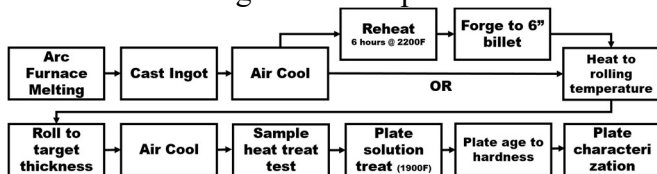


Figure 1: General process flow for production of wrought FeMnAl plate

For successful implementation of this armor steel into a vehicle application, machining and welding

parameters need to be developed. Results from preliminary welding trials on small scale plate with commercially available welding consumables are discussed, as well as observations from machining.

The paper is organized as follows: primary lessons learned from each industrial pour, results from rolling and forging, heat treatment results, welding practices and characterization, and machining practices.

INDUSTRIAL POUR – SEPTEMBER 2016

All pours were conducted by Ellwood Quality Steels (EQS), in New Castle, PA using an eccentric bottom tapping (EBT) electric arc furnace, and ingots were bottom poured. During this first industrial heat, four 12”x54” ingots were successfully cast. One of these ingots is shown in Figure 2.



Figure 2: As-cast ingot of FeMnAl steel produced with high silica teeming flux

Two additional ingots froze off and did not fill, so remaining hot metal was top-poured into 2 ‘emergency’ molds; a 30” tapered ingot and a short 34”x47” ingot. While P and S levels were successfully controlled, the amount of aluminum was below the target. Two teeming fluxes were used for this effort: one with a high carbon content,

and another standard steel flux with high SiO₂ content (>50%). The high SiO₂ content lead to the teeming flux reacting with the molten metal, reducing the aluminum to become alumina (Al₂O₃). [5] Consequently, the total wt% aluminum in the alloy was below threshold levels for successful age hardening behavior, showing now change in Brinell hardness after 30+ hours of ageing time. Aluminum is critical to the formation of the carbide that drives hardness in this alloy. Additionally, the superheat was deemed insufficient for smooth rise of the liquid metal in the mold.

INDUSTRIAL POUR- JULY 2017 & FEBRUARY 2018

Based on the low aluminum issues leading to poor hardening in the first industrial heat, the second heat focused on identification of a teeming flux chemistry compatible with this alloy system. A second goal of this pour was to test an increased super heat. Five ingots were poured: four 12”x54” molds and one 34”x47” mold were used. Each of the four smaller ingots used a different teeming flux: a repeat of the previous, along with a 1:1 lime: alumina flux, and two soda lime alumina + CaF fluxes, with differing amounts of CaF and Na₂O. The second of the soda lime alumina fluxes was specifically formulated for this effort. The composition of the fluxes aimed to drive the melting point down slightly relative to the



Figure 3: As-cast ingot surfaces resulting from a variety of fluxes used, with improving surface quality from left to right in the figure.

commercially available soda lime alumina blend. A comparison of as-cast ingot surfaces is presented in Figure 3.



Figure 4: Fracture surface of a 34”x47” ingot that failed during solidification and cooling.

The standard SiO₂ flux on the far left shows the poor surface from the first industrial heat. The remaining images are ordered from left to right by increasing surface quality of the as-cast ingot, with the best performance from the flux developed specifically for this effort.

While the surface finishes were improved, the 34”x47” ingot fractured due to a combination of thermal and bending stresses upon cooling. The fracture surface of this ingot is shown in Figure 4.

No specific defects were identified within the ingot. The crack path indicates the failure began from the bottom of the ingot halfway between the two supports during cooling, where maximum bending loads would be experienced. This failure mode was noted by the mill to be a known issue with other high alloy steels, such as tool steels. While there was interest in this ingot size for the largest wrought plate thicknesses, it is anticipated that all plate production needs for the future could be met with the 12” ingots successfully poured, which still offer a 3X reduction for 4” thick plates.

February 2018

The best results from the second industrial pour were pulled forward. Repeatability of pouring method was successfully demonstrated in the February 2018 pour. One ingot showed minor solidification cracking on the face attributed to rapid rise in the mold, but this defect was successfully removed via grinding before forging. This will be mitigated in future heats by slowing the rate of rise in the mold through either increased simultaneous molds filled or flow throttling. During this pour, the position of the flux within the mold was also tested, with the flux on the bottom in 3 of 6 molds, and hung at varying heights in the remaining 3. No noticeable effect was observed in surface finish. However, during rolling of the as-cast ingots, several ingots showed evidence of internal voiding. It was determined that these ingots had all had flux hung part way up in in the mold, rather than dropped to the bottom. Hung flux is typically done to ensure fresh flux material is available late in the teeming. In future efforts, the simpler bottom-only flux method will be used.

The measured ingot chemistries are presented in Table 1.

Table 1: Measured ingot chemistries for industrial heat by either wet chemistry of optical emission spectroscopy (OES)

Pour Date	Mn	Al	C	Mo	Si	Fe (bal)
July 17 (wet)	28.8	9.1	1.01	0.5	0.6	59.9
July 17 (OES)	29.19	9.9	0.92	0.5	0.96	58.53
Feb 2018 (OES)	29.7	9.6	0.84	0.54	0.8	58.2

Chemistries for both pours were measured via optical emission spectroscopy (OES) at EQS during ladle refinement. An additional set of measurements for the July 2017 pour were determined with standard wet chemistry methods. The accuracy of OES is known to be affected in high Mn, high Al steels due to the overlap of certain

peaks in the spectrum. Comparing the wet chemistry and optical emission results for the July 2017 pour, OES slightly overestimates the Mn and Al content, and slightly underestimates carbon. As part of the ultimate maturation of the manufacturing process, calibrated standard for OES or spark spectroscopy of this alloy should be developed. Additional wet chemistry results as a function of ingot location are pending.

ROLLING AND FORGING RESULTS

In the production of wrought plate, there are several strategies for converting ingots to plate of the desired thickness. The simplest technique is rolling straight-away. Other more slightly complex processes include cross-rolling, conversion rolling, and forging of the billet prior to hot rolling. Both cross-rolling and forging have been pursued as potentially promising manufacturing paths. In future work, continuous cast slabs may be investigated as a way to enable straight-away rolling without additional conversion steps required.

This alloy system presented challenges during the rolling process. Due to the high aluminum content, and the possibility of segregation during solidification of the ingot, there were concerns about the possibility of intergranular liquefaction during the rolling. Accordingly, a conservative rolling temperature of 1950°F (1065°C) was initially selected to avoid this possibility.

First rolling results were unsuccessful: the ductility of FeMnAl steel is decisively sensitive to rolling temperature. Figure 5 shows the results of this rolling attempt at 1950°F.



Figure 5: Ingot after rolling attempt at 1950°F showing substantial transverse tearing after minimal reduction

The remaining ingots were paused, and taken from the soaking pit for reconditioning. One of these ingots was then forged, and one left in the as-cast condition. The failed ingot was sectioned for chemical analysis and microstructural examination to evaluate the segregation of the as-cast ingot.

The forged billet was later rolled at 2128°F (1165°C), shown in Figure 6.



Figure 6: Forged billet rolled to 0.5" thick plate at a soaking temperature of 2128°F. Plate is ~ 6' wide.

Most recently, billets were rolled at 2200°F (1204°C). Billets were forged to width such that straight-away rolling was possible to minimize heat loss. For the two billets with a target of 0.5", cross-rolling was still necessary, and pieces were reheated between rolling to width and final rolling. This higher temperature resulted in a dramatic decrease in edge cracking compared to previously produced plates from billets, with cracks only 0.5"

deep instead of previous attempts where cracks ran 4-6" deep.

Forging and temperature also have a noticeable impact on surface quality. Figure 7 compares a piece rolled to 1.5" at 1950°F (right), and a piece first forged, the rolled at 2150°F (left).

A more direct comparison of forging versus rolling as-cast was performed with a rolling temperature of 2200°F, with material from the Feb 2018 industrial pour. Figure 8 shows surfaces and edges from the forged billet and the as-cast ingot. In both cases, edge cracking was reduced from previous efforts. The surface finish and edge cracking was still best on the forged material. During rolling of the as-cast ingots, defects occurred which are likely due to voids in the ingot,



Figure 7. Comparison of surface quality of (left) forged and rolled at 2150°F, and (right) rolled at 1950°F plate from the same pour

such as centerline piping.



Figure 8. Plate rolled at 2200F from (left) forged billet and (right) as-cast ingot, showing overall surface quality and edge cracking

HEAT TREATMENT RESULTS

Once material is rolled to plate, proper heat treatment is critical to achieving hardness and impact toughness performance. FeMnAl steel is primarily austenitic, with κ -carbides forming to impede dislocations and increase hardness. [6] To this end, material is first solution treated and quenched, followed by an extended ageing period. This first dissolves any residual carbides and fully austenitizes the system, and then controls nucleation and growth of desired carbides. The 1.5" plate rolled from the as-cast ingot was aged at 1000°F (538°C) in both the as-rolled condition, and after a 2 hour solution treat and quench (STQ) at 1922°F (1050°C). Figure 9 shows the hardness as a function of ageing time for this plate.

To evaluate possible segregation effects, pieces were taken from the top and bottom of the 0.5" plate rolled from billet. As this billet was one of two made from the original ingot, this represents the original bottom and center of the ingot in question. Two different solutionizing times were chosen, since the thinner plate was expected to fully reach temperature sooner. As seen in Figure 10, a shorter solutionizing time resulted in a significantly shorter ageing time required to achieve the target hardness of 330 BHN.

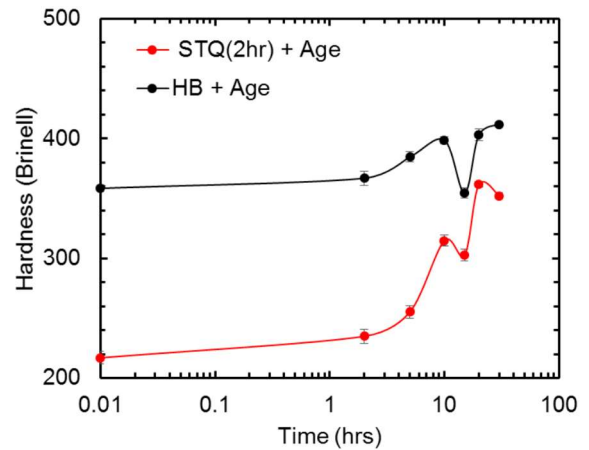


Figure 9. Hardness (Brinell) as a function of ageing time for a 1.5" plate as-rolled (HB) and after solutionizing (STQ)

The microstructure in the as-rolled plate displays the expected grain elongation. After solutionizing, the grain structure is equiaxed, and grain size is significantly increased. Figure 11 shows a microstructure after 30 hours of ageing, with some visible κ -carbide precipitates forming both homogeneously within the grain and at the grain boundary in the 0.5" plate.

The homogeneously formed precipitates are preferred, but the grain boundary carbides largely dominate. However, only two phases are seen, as expected.

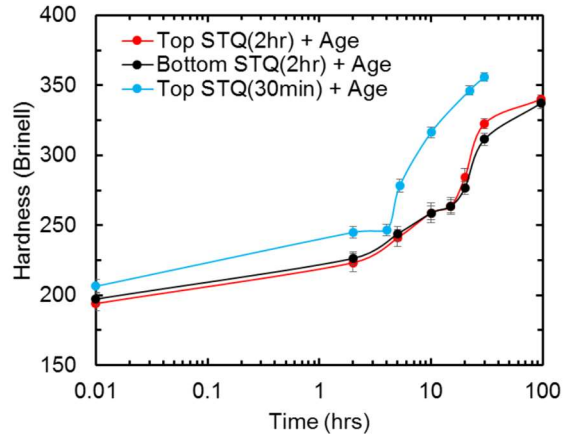


Figure 10. Hardness (Brinell) as a function of ageing time and solutionizing condition for a 0.5" plate

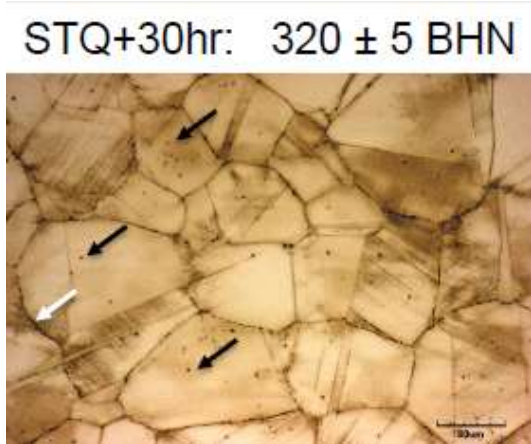


Figure 11. Microstructure of 0.5” plate STQ (2hrs), aged 30 hrs. Black arrows indicate possible homogenously precipitated carbides, while white arrows indicated grain boundary carbide. Scale bar 80 μ m.

One additional issue with heat treatment is the risk of decarburization. In this alloy system, the loss of carbon can de-stabilize the austenite phase, resulting in the formation of ferrite. This is detrimental to the mechanical performance, as the ferrite phase is softer than the austenitic phase. A series of samples of a cast FeMnAl alloy of the same target composition were held in an open-atmosphere over at 2012°F (1100°C) for up to 17 hours to explore the rate of decarburization. Figure

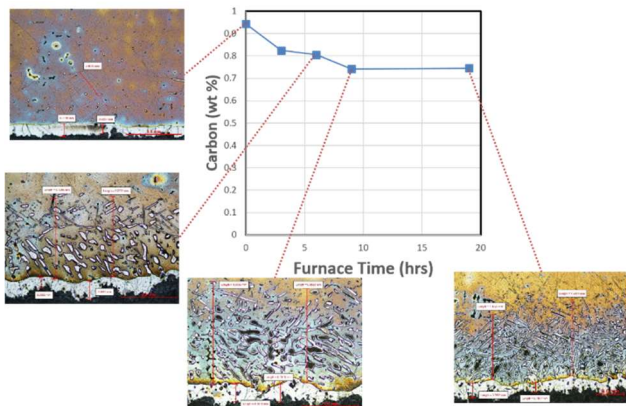


Figure 12. Formation of ferrite during the progression of decarburization in a cast FeMnAl alloy, with a maximum observed depth of 1.3mm

12 shows the measured carbon and the corresponding microstructures for each time measured.

The bright white ferrite layer forms rapidly, with additional grains of ferrite forming up to a depth of 1.3mm (0.05”). Carbon in the sample dropped from 0.93 to 0.75 wt%. However, as expected, the rate of diffusion limits the total amount of carbon lost and the overall depth of the decarburized layer. This ferrite microconstituent is softer than the austenite matrix, which could have potentially detrimental effects on ballistic performance.

WELDING RESULTS

Preliminary welding trials were conducted by TARDEC’s Center for Systems Integration (CSI) using wrought plate produced via Vacuum Induction Melting (VIM) by Sophisticated Alloys. A commercially available 316LSi austenitic stainless steel filler wire was selected. Additional wires are in progress. The joint configuration was a double vee groove, shown in Figure 13.

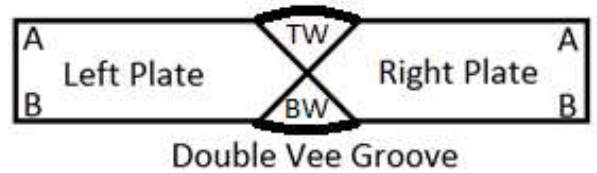


Figure 13. Double vee groove schematic

Charpy and tensile samples were taken from the welded plate, with tensile samples taken from the fusion zone and base plate, and Charpy samples taken from the fusion zone, heat affected zone (HAZ) and base plate. The layout of these samples

relative to the weld is shown in Figure 14.

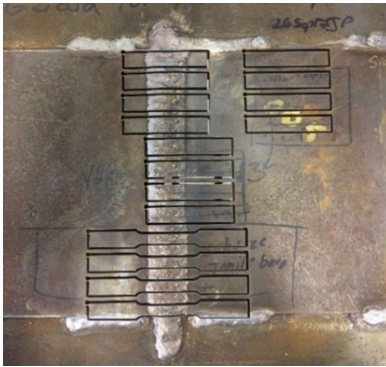


Figure 14. Layout of test samples on welded plate

Charpy Results

Specimens for Charpy testing were machined subsized from the ASTM E23 standard dimensions: therefore, trends, rather than absolute values, are discussed here. Absolute values should not be directly compared to other testing. Typical specimen cross-section was 7.5mmx10mm. Samples were tested at -40°F.

The base metal showed substantially reduced performance relative to the HAZ or weld material: the base metal had an average breaking energy of 8.9J, the weld center had an average breaking energy of 41.1J, and the HAZ had the highest breaking energy, of 73.0 J. This trend in breaking energies is reflected in the characteristic fracture surface of the three areas, shown in Figure 15.

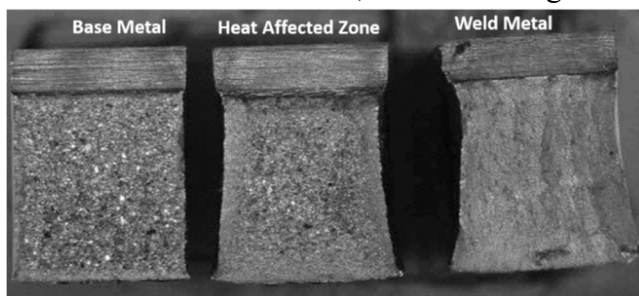


Figure 15. Fracture surfaces of Charpy impact test specimens following impact at -40°F for (left) base metal, (middle) heat affected zone and (right) weld metal

The base metal sample shows brittle intergranular fracture. The heat affected zone demonstrates a more mixed failure mode, with an initially ductile

fracture transitioning to a brittle failure. The weld metal underwent a fully ductile failure. Further work to understand the root cause of the poor base metal impact toughness is ongoing.

Tensile Results

Three tensile specimens were taken through the plate thickness. Tensile curves for the base metal are presented in Figure 16. The elastic modulus was measured at 131 MPa for all specimens, with no systematic variation between the plate faces and core. However, the ultimate tensile strain and total elongation showed a distinct difference between the center and the face: the center samples are shown in red, with faces in green and blue. Strain to failure or center samples ranged from 40%-50%, while faces ranged from 50%-65% total elongation. This is believed to be due to the residual stress state of the wrought plate from the rolling process. Further work regarding residual stress in these materials is ongoing.

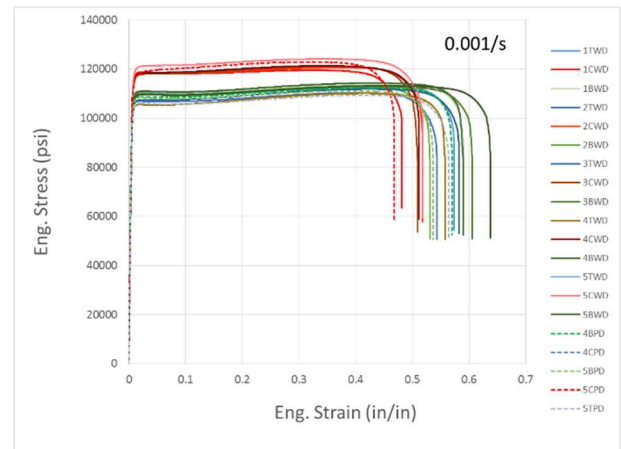


Figure 16. Tensile specimen data for 1'' wrought FeMnAl plate produced in VIM. Plate faces are in blue and green, center samples in red.

The yield strength versus the elongation at failure for both welded and base metal samples are shown in Figure 17. Elastic moduli were similar across all samples and are hence not shown.

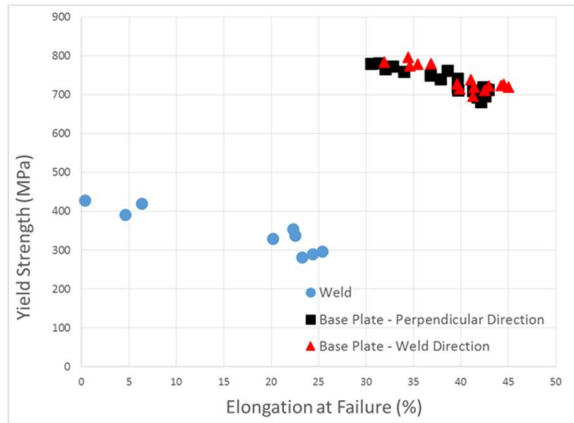


Figure 17. Tensile results for welded samples (blue circles) and base metal (black square – perpendicular, red triangle – parallel), showing yield strength versus elongation at failure

The welded samples showed a systematically lower yield strength, as expected from the filler metal properties. There was also more variance in the total elongation at failure, with several welded samples failing prematurely. All weld tensile specimens failed within the fusion zone. Post-testing examination of the fractured samples showed 2 of twelve samples with a small tear at the interface between the fusion zone and base metal, shown in Figure 18.



Figure 18. Tensile specimen post-testing showing small tear at the interface between the fusion zone and base metal.

While radiography showed full fusion, microstructural analysis showed an unmixed type region at the edge of the fusion zone.

Welded Microstructure

Samples of the welded FeMnAl plate were mounted and polished to a 1µm diamond finished, and etched with 5% Nital, shown in Figure 19. Due to the stainless steel filler metal, this etchant had little effect on the weld metal, and hence grain structures are not obvious. Polarizers were used to help identify grain boundaries.

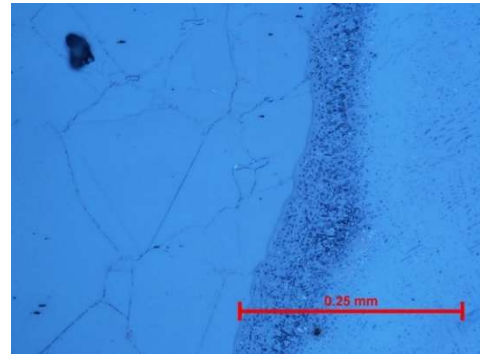


Figure 19. ER 316L filler on cast FeMnAl base plate

There are large grains visible, typical of the heat affected zone. However, the numerous, small pores in a band between the fusion metal and base metal are less expected. To better understand this region, the sample was examined by scanning electron microscopy (SEM) and energy dispersive spectroscopy (EDS). Results are shown in Figure 20.

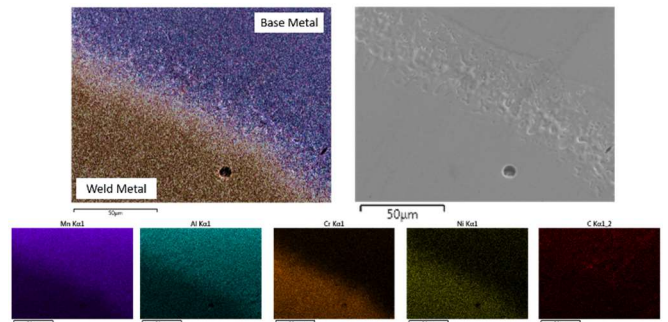


Figure 20. ER 316L filler on cast FeMnAl base plate with (upper left) composite EDS map, (upper right) SEM image (lower purple) Mn concentration (lower teal) Al concentration (lower orange) Cr concentration (lower yellow) Ni and (lower red) C concentration.

Based on the manganese concentration, as well as the chromium content, the porous region appears to

be entirely within the base metal: this is consistent with the hypothesis that this is an unmixed region. It is currently hypothesized that this zone melted during welding, but did not mix with the bead, and then due to system constraints and thermal expansion coefficients, solidification resulted in the formation of voids. Gleeble simulation of the welding process will be undertaken soon to explore this. During welding, the welders commented that the pool did not flow well, another potential hallmark of mixing issues.

Hardness

A microhardness map was prepared via Struers Durascan, with a Vicker’s microindenter. Results are presented in Figure 21. The weld bead is softer than the base metal, as expected, but some softening of the heat affected zone is observed. The boundary zone is not obviously visible in this particular analysis, despite concerns about the mechanical properties of that region. Further detailed hardness mapping of the porous region is planned for future work.

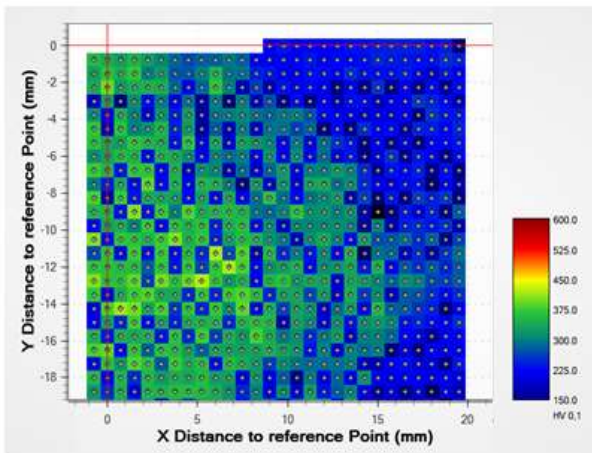


Figure 21. Vicker’s hardness map of double vee groove weld bead and heated affected zone of ER 316L filler on cast FeMnAl base plate with weld bead to the right of the image. Image scale is from 150HV to 600HV.

MACHINING RESULTS

During the preparation of the plate for welding, a 3D machining operation was performed to prepare

the double vee groove. The cutting tool used was brand new, and retained for post-analysis. Stereoscopic images of the cutting bit and swarf are presented in Figure 22.



Figure 22. Stereoscopic images of (top) the cutting bits in the used (leftmost) and unused (center) bits, and the produced cutting swarf (bottom)

As somewhat expected from the high-work hardening nature of high Mn steels, significant tool wear was observed in a relatively low number of linear feet machined. The leftmost object in Figure 22 shows nicks and wear compared to the unused tool to its right. Further optimization of cutting parameters is ongoing.

The machining by-product was more chip-like, without long, continuous pieces. This chip is more typical of a cast iron than a steel, but well within the ability of a typical shop to manage.

FUTURE WORK

Significant basic and applied research remains to be completed in this project. Currently underway are efforts to characterize the fatigue performance, hydrogen embrittlement susceptibility, Gleeble simulation of heat affected zone formation, thermomechanical simulation of hot ductility and out of position welding.

CONCLUSIONS

Wrought FeMnAl plate was successfully produced using common, commercially viable large scale practices. Initial results also show promise for weldability and machinability of this material. Further optimization of heat treatment, welding and machining practices is required, as well as additional characterization of industrially-produced plate.

ACKNOWLEDGMENTS

The information, data, or work presented herein was conducted as an Advanced Vehicle Power Technology Alliance (AVPTA) "Extended Enterprise" project funded by the U.S. Army Tank Automotive Research, Development and Engineering Center (TARDEC), U.S. Department of Defense (DoD), Department of the Army. AVPTA is Chartered under the auspices of the Department of Energy / DoD Memorandum of

Understanding titled "Concerning Cooperation in a Strategic Partnership to Enhance Energy Security "DoD-DoE AVPTA, with additional funding from Army ManTech "Manufacturing Processes for Lightweighting Heavy Combat Vehicles". We also thank Fred Fletcher, Jim Kane, Joe DeGenova and Daniel Field for their contributions to this project. Thanks to TARDEC CSI for welding the first test samples.

REFERENCES

- [1] US Army PM Abrams, *Abrams Special Topic: Transportability IPT Briefing*, 2015.
- [2] R. Howell and J. Montgomery, *Advancements in Steel for Weight Reduction of P900 Armor Plate*, Survivability Materials Branch ARL, 2008.
- [3] R. A. Howell, *Microstructural Influence on Dynamic Properties of Age Hardenable FeMnAl Alloys*, Rolla: Missouri S&T, 2009.
- [4] K. Sebeck, R. Gerth and R. Thyagarajan, "Abrams Weight Reduction Study," TARDEC Report #29078, Warren, 2017.
- [5] Y.-B. Kang, M.-S. Kim, S.-W. Lee, J.-W. Cho, M.-S. Park and H.-G. Lee, "A Reaction Between High Mn High Al Steels and CaO-SiO₂-Type Molten Mold Flux: Part II. Reaction Mechanism, Interface Morphology, and Al₂O₃ Accumulation in Molten Mold Flux," *Met. Trans B*, vol. 44B, p. 309, 2013.
- [6] O. Zambrano, "A General Perspective of Fe-Mn-Al-C Steels," Arxiv Cond-Mat 1707.01920, 2017.